Design Rules for Quantum Imaging Devices: Experimental Progress Using CMOS Single Photon Detectors♦

Edoardo Charbon, Neil J. Gunther, Dmitri L. Boiko, Giordano B. Beretta
Digital Printing and Imaging Laboratory
HP Laboratories Palo Alto
HPL-2006-117
August 14, 2006*

CMOS, detector arrays, interferometer, phase twinning, quantum imaging, SPAD (single photon avalanche diode)

We continue our previous program where we introduced a set of quantum-based design rules directed at quantum engineers who design single-photon quantum communications and quantum imaging devices. Here, we report on experimental progress using SPAD (single photon avalanche diode) arrays of our design and fabricated in CMOS (complementary metal oxide semiconductor) technology. Emerging high-resolution imaging techniques based on SPAD arrays have proven useful in a variety of disciplines including bio-fluorescence microscopy and 3D vision systems. They have also been particularly successful for intra-chip optical communications implemented entirely in CMOS technology. More importantly for our purposes, a very low dark count allows SPADs to detect rare photon events with a high dynamic range and high signal to noise ratio. Our CMOS SPADs support multi-channel detection of photon arrivals with picosecond accuracy, several million times per second, due to a very short detection cycle. The tiny chip area means they are suitable for highly miniaturized quantum imaging devices and that is how we employ them in this paper. Our quantum path integral analysis of the Young-Afshar-Wheeler interferometer showed that Bohr's complementarity principle was not violated due the previously overlooked effect of photon bifurcation within the lens—a phenomenon consistent with our quantum design rules—which accounts for the loss of which-path information in the presence of interference. In this paper, we report on our progress toward the construction of quantitative design rules as well as some proposed tests for quantum imaging devices using entangled photon sources with our SPAD imager.

* Internal Accession Date Only
♦ Published in Proceedings 6305 of Optics & Photonics: Quantum Communications and Quantum Imaging IV, San Diego, CA, 13-17 August 2006. Approved for External Publication

Design Rules for Quantum Imaging Devices: Experimental Progress Using CMOS Single Photon Detectors

Edoardo Charbon[a], Neil J. Gunther[b], Dmitri L. Boiko[a] and Giordano B. Beretta[c]

[a]Ecole Polytechnique Fédérale de Lausanne (EPFL), Lausanne, Switzerland
[b]Performance Dynamics, 4061 East Castro Valley Blvd., Castro Valley, California, USA
[c]HP Laboratories, 1501 Page Mill Road, Palo Alto, California, USA;

1. INTRODUCTION

Previously,[1] we proposed to develop a set of design rules (DRs) suitable for application by engineers when designing and fabricating quantum imaging and quantum communication devices. These DRs are based on Feynman's path integral representation of quantum mechanics applied specifically to photonics (something Feynman himself did not present in his book[2]). Failure to adhere to our DRs can lead to serious design errors, and we revealed one such flaw in the design of the Young-Afshar-Wheeler (YAW) interferometer; a quantum imaging device which has been used to claim that both the *particle* and the *wave* nature of the photon could be measured simultaneously, in violation of Bohr's complimentarity principle.[3] The error is associated with a form of photon *bifurcation*; a purely quantum effect which is encompassed quite naturally within our DRs but has heretofore been overlooked.

The key goals of our research program are twofold:

1. Elevate our quantum DRs to a more serviceable quantitative engineering level
2. Test the DRs against actual quantum devices using entangled photon sources and our silicon-based single photon detectors

To achieve both of these objectives requires a modern laser system. To this end we formed a team based in the School of Computer and Communication Sciences in the Ecole Polytechnique Fédérale de Lausanne (EPFL), Switzerland where we have just installed a state-of-the-art femtosecond laser system and are now in the process of designing experiments to quantify and test our proposed DRs.

The structure of this progress report falls into two principal parts: Section 2 presents an update on our *theoretical* understanding, while Section 3 presents an update on our *experimental* progress. In Section 2.2, we restate and report on the development of our quantum DRs. Section 2.4 presents our recent progress in numerical simulations of the quantum path integral. Section 2.3 discusses our deeper understanding of the photon bifurcation process,[1] and in Section 2.5 we elaborate on the quantum path integral represenation of entangled biphotons. Section 3.1 describes the capabilities of our femtosecond mode-locked laser which will be used for both single photon and entangled photon validation of our DRs. Section 3.2 describes our unique capability for detecting single photons using VLSI arrays fabricated in CMOS technology. Section 4 outlines the next steps in our research program.

Further author information: (Send correspondence to N.G.)
E.C.: E-mail: edoardo.charbon@epfl.ch, Telephone: +41 21 693 6487
N.G.: E-mail: njgunther@perfdynamics.com, Telephone: +1 510 537 5758
D.B.: E-mail: dmitri.boiko@epfl.ch, Telephone: +41 21 693 8145
G.B.: E-mail: giordano.beretta@hp.com, Telephone: +1 650 857 6713

2. THEORETICAL PROGRESS

In this section, we report on progress in our theoretical understanding of developing photonic DRs for quantum imaging and communication devices.

2.1. Quantum Path Integral

Any trajectory $x(t)$ that can be taken by a physical photon between its source (s) and a detector (d) corresponds to a complex quantum amplitude:

$$\phi[x(t)] = A \exp\left(\frac{i}{\hbar} S[x(t)]\right) \tag{1}$$

where A is a normalization constant. The phase of (1) is determined by the classical action

$$S[x(t)] = \int_{t_s}^{t_d} L(x, \dot{x})\, dt \tag{2}$$

where $L(x, \dot{x}) = T(\dot{x}) - V(x)$ is the Lagrangian for a point-particle with kinetic energy T and potential energy V, located at position x at time t and moving with velocity $\dot{x} = dx/dt$. The complete quantum propagator for the photon is a functional integral:

$$G(d|s) = \int_{s}^{d} \phi[x(t)]\, \mathcal{D}x(t) \tag{3}$$

corresponding to a summation (*superposition*) over all paths between s and d with $\mathcal{D}x(t)$ the appropriate integration measure. Eqn.(3) is the *quantum path integral* (QPI).[1, 2, 4]

We have already applied (3) to the scalar approximation for the photon and shown that it is the Green's function for the relativistic Klein-Gordon equation,[1] with the time-independent case further simplifying to the optical Helmholtz equation.[5] As we explain in Sect. 2.4, this scalar approximation is also consistent with Fourier optics[6] and sufficient for analyzing many quantum imaging designs. Polarization effects can also be included by requiring that (3) satisfy the vector Maxwell-Lorentz equations. Finally, a more detailed analysis of the interaction between photons and electrons (material) demands the application of the fully Lorentz-covariant Green's functions of quantum electrodynamics.[7] In other words, a consistent quantum theory of the photon is available to us at different levels of approximation within the same formalism.

The quantum amplitude (1) can also be regarded as a complex vector (denoted by $\nearrow$ hereafter), called a *phasor*,[6] which rotates with frequency $\omega = 2\pi c/\lambda$ as it traverses the path $x(t)$ and whose length represents its magnitude. We employ this phasor concept in Sect. 2.3.

2.2. Design Rules

The goal for our DRs is to enable engineers to construct quantum imaging and communication devices that are *correct by design*. Currently, our DRs are formulated at the quantum level of the photon, which are *topologically* correct. The purpose of engineering DRs is to abstract away the physics while leaving the designer with the correct *geometrical* guidelines in terms of tolerances, rules-of-thumb, etc. To reach this goal, we require the experimental system described in Sect. 3 to be fully operational. The current topological quantum-level DRs[1] may be summarized as:

1. **Path Rule:** The physical photon is neither a infinitesimal "billiard ball" nor a *wave*. It is the collection of QPI paths defined in (3).

2. **Interaction Rule:** Photons do *not* interact with photons. Photons only interact with electrons via *events* (see Rule 4). The QPI paths in the diagram for Rule 5, for example, do not belong to two photons but the same single photon.

3. **Material Rule:** Introducing *any* material into a given optical device automatically introduces electrons which can potentially cause new events ($\mathcal{E}$).

4. **Event Rule:** An *event* $\mathcal{E}$ is an interaction between a photon and an electron (e.g., absorption or emission). Detection (i.e., photoabsorption) is the *final* event. Between events the photon is *free* of interactions.

5. **Sum Rule:** Alternative QPI paths are *OR*-ed to give simple superposition (cf. eqn. 3):

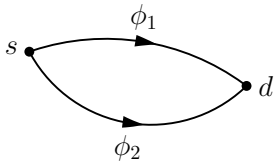

$$G(d|s) \equiv \phi_1 + \phi_2$$

6. **Product Rule:** QPI path dependencies are *AND*-ed:

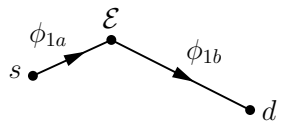

$$G(d|s) \equiv \phi_{1a} \cdot \phi_{1b}$$

7. **Convolution Rule:** This rule tells us how to combine QPI rules 5 and 6 to produce the quantum superposition of segmented paths:

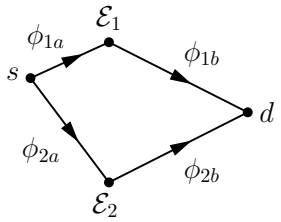

$$G(d|s) \equiv (\phi_{1a} \cdot \phi_{1b}) + (\phi_{2a} \cdot \phi_{2b})$$

8. **Detection Rule:** Only *real-valued* numbers can be compared with physical measurement at a detector. Such a real number corresponds to the probability:

$$\Pr(d) \equiv \overline{G(d|s)}\, G(d|s)$$

of finding a single photon at the detector location d.

As part of gaining a deeper understanding of these rules, we can now underscore the following important points. First, these DRs mean there is no longer any need for a designer to make the usual distinction between *amplitudes* and *intensities*, as is often required by conventional (wave) optical analysis. In the QPI formalism of the single photon, we always work with photon amplitudes. Second, Rule 4 appears surprising in that we never need to define the explicit form of the (instantaneous) interaction between a photon and matter. It is quite legitimate, however, in that the QPI path segmentation corresponds to momentum exchange between the photon path and the material, and this is logically equivalent to defining a transition or scattering matrix.

2.3. Phase Twinning

We previously analyzed the YAW interferometer[3] (Fig. 1) by applying the DRs of Sect. 2.2 and found that the design error could be attributed to a quantum effect we termed *photon bifurcation*[1]; an effect that causes which-way (WW) path information to be lost in the presence of interference, completely in accordance with conventional quantum theory and Bohr's complementarity principle.[8–10] More recently we have developed a simpler and, we believe, less ambiguous explanation in terms of QPI *phase twins*.

The two pinholes 1 and 2 on the left of Fig. 1 produce observable interference fringes on a screen placed at σ_1. If that screen is removed and replaced with a suitable convergent lens L, the two pinholes can be focused as (inverted) image spots $2'$ and $1'$ respectively on a plane positioned further along the optical axis at σ_2. The

wire grid (WG) is merely used to convince the reader that interference is still present even though fringes are no longer observable.[3] The remainder of the original analysis essentially relies on classical geometrical optics (shown as solid and dashed arrows in Fig. 1) to explain how the image spots due to wavefunctions ψ_2' and ψ_1' form at σ_2. It is (incorrectly) concluded that WW paths $\psi_1 \to \psi_1'$ and $\psi_2 \to \psi_2'$ can be determined in the presence of interference; a claim which stands in complete contradiction to the complementarity principle which disallows the simultaneous measurement of particle (WW path) and wave (interference) properties of the photon (or any quantum particle). But precisely where is the flaw?

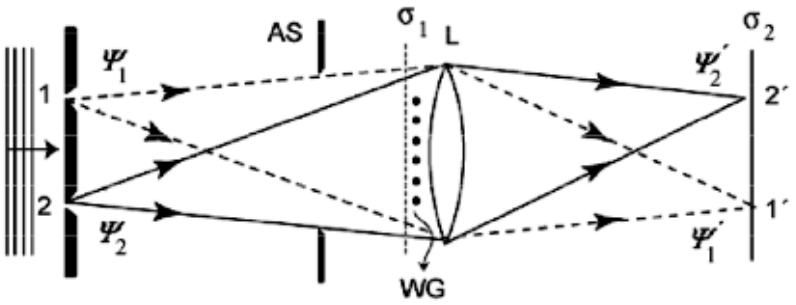

Figure 1. Ray optics analysis of YAW[3] which disregards the DRs in Sect. 2.2.

To facilitate our phase-twinning explanation, we employ the phasor representation of QPI paths described in Sect. 2.1. In the QPI formulation, a single photon can propagate along any and all paths between source and detector. This is one way to visualize the weird distinction between a classical particle taking the unique path which minimizes the action (2) and a quantum entity like the photon which takes all possible paths. What matters more than a photon QPI path is its phase relative to other QPI paths when it reaches the detector (i.e., the final event). Pairs of relative phases are shown as phasors (*blue arrows*) in Fig. 2. Only closely aligned phasors contribute significantly to the measured intensity according to Rule 8. We can think of these phasors as being like *identical* twins, whereas mismatched phasors are like *fraternal* twins; they arrive together but their orientations are not aligned.

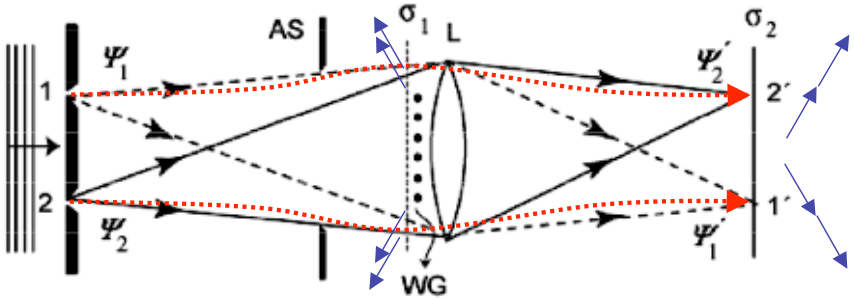

Figure 2. Quantum-path twinning represented by phasor pairs (*blue arrows*) at image planes σ_1 and σ_2.

The design flaw stems from a failure to recognize that every classical ray path in Fig. 1 has an associated twin QPI quantum path coming from the other source. Examples of two such non-classical paths are shown as (exaggerated) red dotted lines $1 \to 2'$ and $2 \to 1'$ in Fig. 2. For simplicity, consider only paths arriving at detector $2'$; recognizing that by symmetry the same arguments will hold for detector $1'$. In particular, consider just the classical path $2 \to L \to 2'$ along with the non-classical QPI path $1 \to L \to 2'$. Further suppose that these two paths correspond to a fringe *maximum* at σ_1 (when it was in position) i.e., their phasors must have been closely aligned at that point in order to produce constructive interference. With σ_1 removed, the two phasors will continue to rotate but they must remain aligned with each other even as they propagate more slowly in the

glass ($n_g \sim 1.5$) lens at L. Thereafter, both optical paths are identical up to the detector at $2'$, so the twin phasors will have rotated into a different orientation but still be aligned. Since they arrive as identical phase twins, they contribute vectorially (i.e., added head to tail) to the measured intensity at detector $2'$ via the square of the *resultant* vector length (Rule 8). Conversely, if the phasors originally corresponded to a fringe *minimum* at σ_1, they must arrive as fraternal twins out of phase by π radians at detector $2'$, and their zero-length resultant vector means they do not contribute to the measured intensity. The case of intermediate fringe brightness can be understood in the same way.

Integrating over all such anterior points near the lens, we find that twice as many QPI paths arrive at each detector as would be expected on the basis of classical optics but half of these phasors cancel each other, so that the intensity distribution at the two image spots matches that at the two pinholes i.e., the energy distribution is invariant. Since each detector receives photons from both sources 1 and 2, the YAW does not violate complementarity. Instead of starting with $2 \rightarrow L \rightarrow 2'$ as the classical path, we could just as well commence with $1 \rightarrow L \rightarrow 1'$ (standard refracted ray) and consider $2 \rightarrow L \rightarrow 1'$ to be its non-standard QPI twin. It is this option in QPI paths that we previously referred to as photon path *bifurcation*.[1]

2.4. Device Simulations

Since the QPI (3) formally contains both scattering and bound-state solutions, manual calculations can present a formidable task. Therefore, any computational aid is welcome. Until recently, however, we only had access to simple QPI simulation tools[11, 12] which are too limited to calculate correct optics for a device like the YAW.

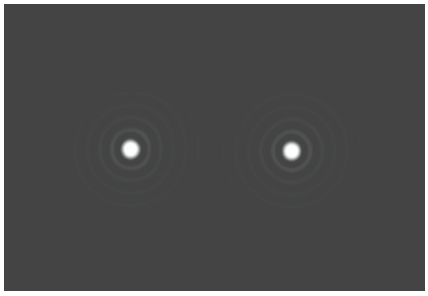

(a) In the absence of the wire grid (WG) in Fig. 2, each image spot exhibits an Airy pattern due to the finite diameter lens (L) acting as a low-pass filter.

(b) With wires (WG) the image spots show slight corruption due either to scattering (diffraction) effects or numerical artifacts.

Figure 3. Numerical simulation of the image plane in the YAW of Fig. 1.

As mentioned in Sect. 2.1, the QPI is a Green's function:

$$\psi(x_2, t_2) = \int G(x_2, t_2 | x_1, t_1)\, \psi(x_1, t_1)\, dx_1 \tag{4}$$

which expresses the transition from an initial quantum amplitude $\psi(x_1, t_1)$ to a final amplitude $\psi(x_2, t_2)$ as a superposition of paths between these amplitudes. Considering the time-independent or steady-state case, and allowing the points x_1 and x_2 to be defined anywhere on the respective two-dimensional planes $\mathbf{x}_1$ and $\mathbf{x}_2$, (4) simplifies to:

$$\psi(\mathbf{x}_2) = \int G(\mathbf{x}_2 | \mathbf{x}_1)\, \psi(\mathbf{x}_1)\, d^2 x_1 \tag{5}$$

where $\psi(\mathbf{x}_1)$ and $\psi(\mathbf{x}_2)$ respectively represent the object and image field amplitudes, similar to those shown in Fig. 2. The QPI propagator $G(\mathbf{x}_2|\mathbf{x}_1)$ is now equivalent to the optical *point spread function* (PSF).[6] With this mapping in hand, we can resort to using more sophisticated numerical simulation tools such as *ImageJ*[13] to calculate the corresponding QPI. As an example, Fig. 3(a) shows the computed image spots in the YAW without the wire grid (WG), while Fig. 3(b) shows the deterioration which may be due to slight diffraction effects from WG or numerical artifacts or both. Improving on this result was not warranted.

2.5. Entangled Biphotons

We have also gained a better understanding of entangled biphotons within the QPI formalism. Essentially, the quantum amplitude for a biphoton can be regarded as a segmented path like that shown in Fig. 4(a). This follows immediately from the fact that the entangled photons are correlated and therefore must have their own propagators viz., G_s for the *signal* photon and G_i for the *idler* photon. Correlation also requires that the Green's function kernel be written as a product $\sim G_s \times G_i$. But this is analogous to the result one would obtain by applying Rule 6 for a QPI path segmented by an interaction event $\mathcal{E}$.

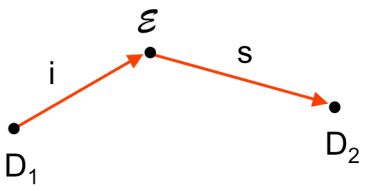

(a) Single QPI amplitude composed of idler and signal path segments.

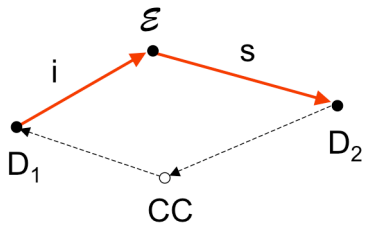

(b) Closed circuit formed by including paths to the coincidence counter.

Figure 4. QPI diagrams for entangled photons where the BBO source becomes the creation event $\mathcal{E}$ which also acts to segment the path between the two detectors.

One can interpret spontaneous parametric down conversion (SPDC) in Fig. 4(a) as being the creation event $\mathcal{E}$ with the signal photon going off to detector D_2, while the idler photon goes backwards in time from detector D_1 to $\mathcal{E}$. Since the photon is its own anti-particle, there is no inconsistency here. Moreover, this interpretation bears a strong resemblance to the *advanced wave* picture due to Klyshko.[14,15] Extending this notion to include the coicidence counter (CC) results in the kind of *closed* circuit shown in Fig. 4(b), whereas the QPI amplitude for a single photon resembles an *open* circuit in that it only requires one detector (cf. Rule 6).

Note that the biphoton QPI and the phase-twinned QPI are completely unrelated. The biphoton involves two path segments *within* the same QPI amplitude, whereas phase twinning involves two *different* QPI amplitudes (for a single photon) that become phase-matched at the same point in space and time.

The closed circuit concept in Fig. 4(b) also provides a natural explanation of quantum ghost imaging.[15–17] Fig. 5 is topologically equivalent to the closed circuit QPI in Fig. 4(b) where the *thin lens* equation:

$$\frac{1}{d_o} + \frac{1}{d_i} = \frac{1}{f}$$

of classical optics holds even though the image is only seen in coincidence counts (ghost). The ghost image effect also occurs no matter on which side of the BBO the lens is placed. In combination with the improved detection

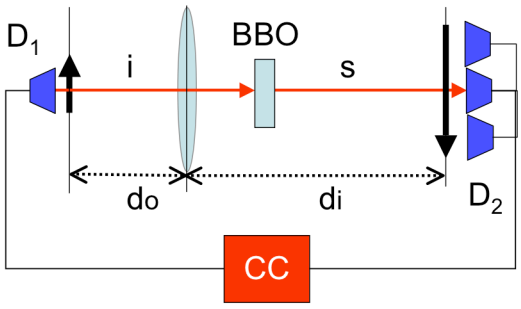

Figure 5. Unfolded representation of a quantum ghost imaging device showing the effective closed QPI circuit.

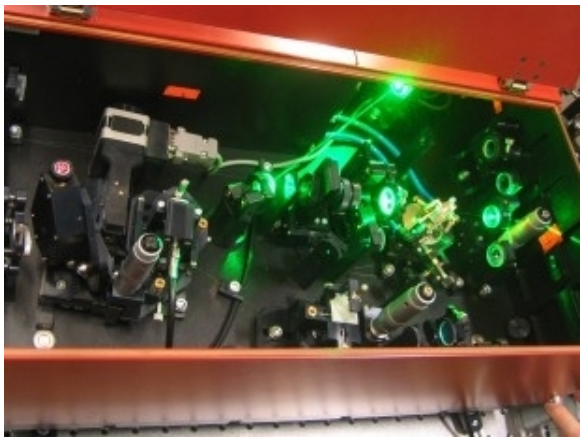

(a) Ti:Sapphire laser cavity with integrated pump system capable of producing femtosecond mode-locked laser pulses.

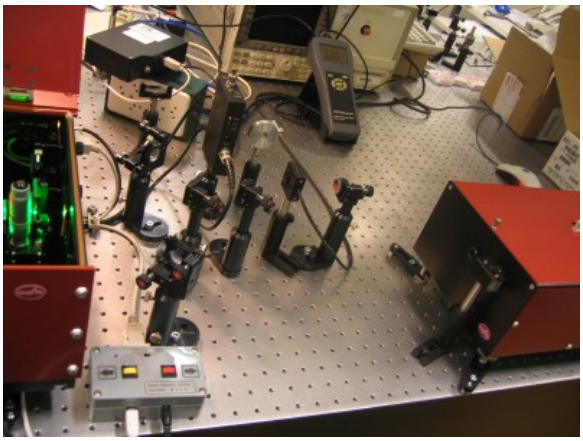

(b) Third harmonic generator (*right*) is pumped by femtosecond laser pulses (*left*). Optical elements (*center*) are used to monitor the mode-locking regime and match the beam waist.

Figure 6. Ti:Sapphire mode-locked laser with frequency tripler (Model TIF-100 Avesta Project, Ltd.).

capability and 1000 times speedup from our SPAD array detectors, all these devices, the YAW, ghost imaging and others involving WW path marking and quantum erasure[8–10] are of interest to us from the standpoint of providing test cases for our geometrical quantum DRs.

3. EXPERIMENTAL PROGRESS

The goal for our DRs is to enable engineers to construct quantum imaging and communication devices that are *correct by design* by progressing from the topologically correct physical rules in Sect. 2.2 to the correct geometrical construction rules. Reaching this objective requires experimental validation.

Experimental verification of the non-classical propagation of photons will be realized by utilizing biphoton states and introducing discrimination in the temporal feedback loop of the classical and QPI paths. Such an experimental arrangement, based on entangled biphotons, requires the use of short and highly intense 100-femtosecond laser pulses. These are used to pump a nonlinear crystal optimized for spontaneous down conversion to create correlated photons pairs (biphoton). The detection part of the experimental setup is based on a conventional coincidence counting scheme implemented for the analysis of the biphoton states. A feature which distinguishes our experimental design from those used in previous quantum imaging devices which have employed single photon detectors and coincidence counting, is a 2D array of SPAD detectors for measuring both temporal and spatial correlations.

3.1. Biphoton Source

As the source of biphotons, we are using SPDC of femtosecond laser pulses in a beta barium borate (BBO) crystal. An optical pulse of about 200 fs width at 267 nm wavelength (the third harmonic of the Ti:Sapphire laser) will be converted into two k-space conjugated photons centered at 534 nm wavelength; the wavelength of maximal quantum efficiency of our Si-based detectors, as described below.

At this stage of development of our experimental setup, we have installed a Ti:Sapphire mode-locked laser system with third harmonic generation (Fig. 6). The Ti:Sapphire laser system is tunable in the range of 740–920 nm and delivers 100 fs pulses at 93 MHz repetition rate. In our experimental setup, it operates at 800 nm wavelength (close to the center of the gain line) providing up to 0.5 W mean optical power. The third harmonic generator provides up to 35 mW of ultraviolet pulses (267 nm wavelength). Since the SPDC process is of low quantum efficiency, until recently, the major effort was focused on achieving the required performance of our CMOS-based

2D arrays of single photon detectors (Fig. 7). We now turn to the details of these detector arrays fabricated in CMOS.

3.2. 2D Single Photon Detectors

Single photon detection on a large scale is made possible by a device known as a *single photon avalanche diode* (SPAD) implemented in CMOS. Essentially, this is a p-n junction (Fig. 9) reverse biased above its breakdown voltage V_{bd}, thus causing it to operate in the so-called Geiger regime. The high electric field across the depletion region causes primary carrier pairs arising from photon absorption to be multiplied by impact ionization. The result of this process is an avalanche current involving thousands of secondary carriers. Since the reverse bias exceeds breakdown, the optical gain achieved by the device is virtually infinite i.e., it sweeps all available carriers across the depletion region.

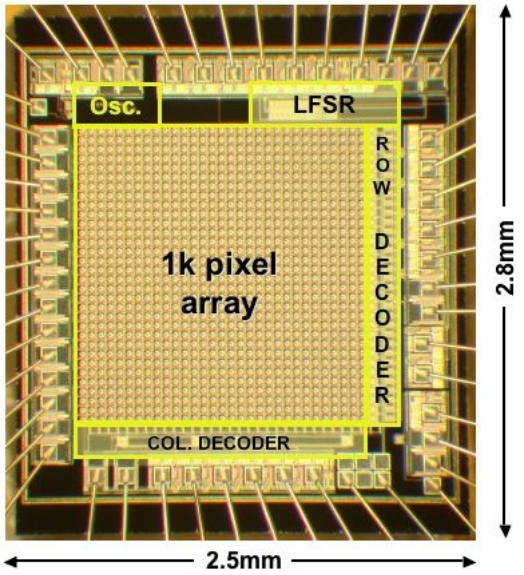

Figure 7. Array of 1024 single photon detectors.

To avoid damaging the p-n junction, it is necessary to *quench* the avalanche. There exist several methods to quench an avalanche both actively and passively. The simplest passive quenching mechanism consists of placing a resistance R_q in series with the p-n junction (Fig 8). When a photon is absorbed the avalanche current I_A forces the voltage across the p-n junction to drop below breakdown, thus removing the conditions that initially caused the avalanche. After quenching, the voltage across the p-n junction must return to the initial value in order to enable detection of the next photon. The duration of this phase, known as *recharge*, is determined by the product $R_q\,C_X$, where C_X is the capacitance seen at the point X in Fig 8. The total time required for quenching and recharge is called *dead time*. During this time the detector is inactive.

Solid-state implementations of SPADs which are not fully-integrated have existed since the 1960s.[18] Silicon implementations have also been demonstrated decades ago,[19] but it is only recently that researchers at EPFL (and elsewhere) have been able to fully integrate SPADs in CMOS technology.[20, 21] The main difficulty with CMOS integration has been the design and optimization of the structures that prevent edge discharge, caused by the high electric field at the corners of the junction. The solution adopted in reference[20] consists of utilizing a combination of deep and shallow wells to force a smooth doping profile at the corner of the junction. Fig. 9 shows a particular variant of this concept.

Another difficulty is to make SPADs compatible with other CMOS circuitry. This requirement is the *sine qua non* for the integration of readout and other critical circuitry on the same chip. The generic SPAD circuit shown in Fig. 10 consists of a reverse biased p-n junction, quenching/recharge circuitry (Q/R in the figure), an avalanche

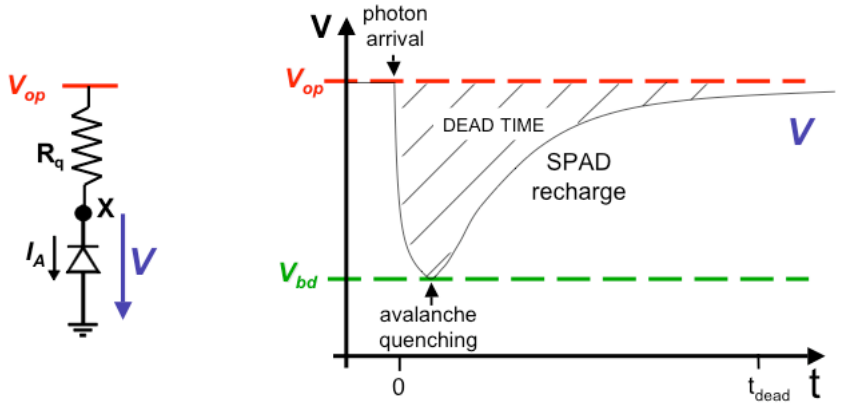

Figure 8. Principle of avalanche quenching and recharge.

detector or a comparator, and readout circuitry (R/O in the figure) with voltage V_{CTRL} to control its operation. The cathode (or anode) potential is made to vary from VDD to approximately zero volts during a detection cycle. This voltage excursion can be captured easily by a simple inverter, provided the proper threshold voltage V_{TH} is chosen. The readout circuit can be as simple as a pass gate, however it may be much more complex and include integrated timing discrimination devices. This compact SPAD design has been proven to be robust, scalable, and compatible with low power systems. It has been integrated in a number of technologies using several readout schemes.[22–25] Fig. 11 shows a photomicrograph of the device implemented in 0.8 μm CMOS technology.[22]

The 2D single photon detector arrays we plan to use in our experiments have two basic requirements:

1. A relatively large number of pixels with small pitch
2. A fast readout scheme to ensure accurate photon timing detection.

The timing accuracy enables precise determination of the coincidence time of arriving photons. Many independently operating pixels allow us to perform a precise determination of the spatial distribution of arriving

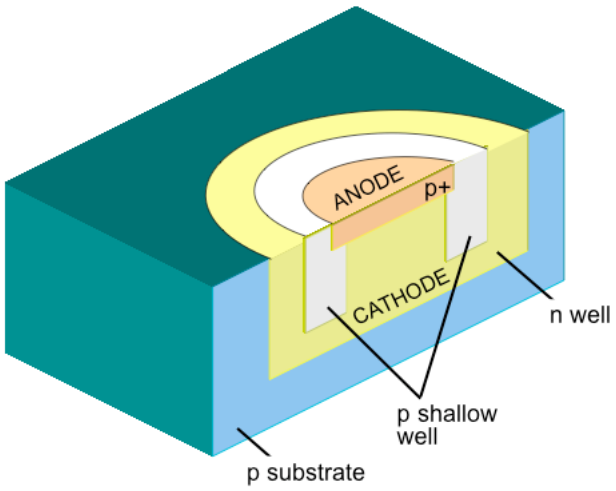

Figure 9. 3D pictorial of CMOS single-photon detector diode showing well structures.

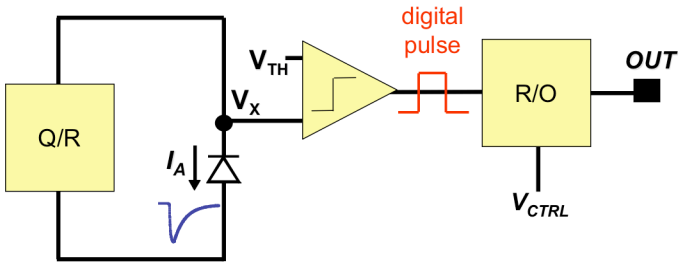

Figure 10. Generic SPAD circuit. It consists of a reverse biased p-n junction, an avalanche detector, and circuitry to perform impedance matching and routing towards the remainder of the imaging system.

photons. The basic architecture of the sensor consists of a matrix of SPADs, a row selection mechanism (or a on-demand selection scheme), a time discrimination layer, an ancillary circuitry for biasing purposes, and a readout block. The time discrimination layer may consists of a battery of time-to-amplitude converters or time-to-digital converters, or simply high-speed counters. Time discrimination may also be performed externally in a separate chip.[23, 26] An example of a simple random access architecture where SPAD outputs may be independently routed to the sensor exterior is shown in Fig. 7. This sensor was fabricated in 0.8 μm CMOS technology with a 2D array of 32×32 independent SPADs.

4. NEXT STEPS

Our primary goal is to develop quantitative DRs for engineers desiging quantum communications and quantum imaging devices. We have a Ti:Sapphire laser with a frequency tripler installed and we are in the process of acquiring BBOs to furnish entangled photon sources using SPDC. In the meantime, other experiments are being considered to exercise our latest generation of SPAD detectors without entangled photons. We plan to report on our results in the near future.

ACKNOWLEDGMENTS

One of us (NJG) thanks H. Gluender for assistance in using ImageJ. Portions of this research were supported by a grant from the Swiss National Science Foundation.

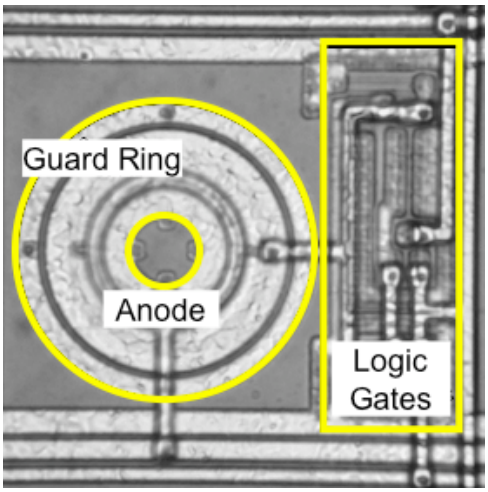

Figure 11. Photomicrograph of a SPAD pixel implemented in 0.8 μm CMOS technology. The pitch is 58 μm in this implementation.

REFERENCES

1. N. J. Gunther and G. B. Beretta, "Towards practical design rules for quantum communications and quantum imaging devices," *Proc. SPIE Int. Soc. Opt. Eng.* **5893**, p. 58930W, 2005.
2. R. P. Feynman and A. R. Hibbs, *Quantum Mechanics and Path Integrals*, McGraw–Hill, New York, 1965.
3. S. S. Afshar, "Violation of the principle of complementarity, and its implications," *Proc. SPIE Int. Soc. Opt. Eng.* **5866**, pp. 229–244, 2005.
4. H. Kleinert, *Path Integrals in Quantum Mechanics, Statistics, Polymer Physics and Financial Markets*, World Scientific, Singapore, 3rd ed., 2004.
5. M. Born and E. Wolf, *Principles of Optics*, Pergamon, UK, 4th ed., 1970.
6. J. W. Goodman, *Introduction to Fourier Optics*, Roberts & Company, Colorado, 3rd ed., 2005.
7. R. P. Feynman, *Quantum Electrodynamics*, W. A. Benjamin, Reading, MA, 1962.
8. M. O. Scully and K. Drühl, "Quantum eraser: A proposed photon correlation experiment concerning observation and "delayed choice" in quantum mechanics," *Phys. Rev. A* **25**, pp. 2208–2213, Apr 1982.
9. P. D. D. Schwindt, P. G. Kwiat, and B.-G. Englert, "Quantitative wave-particle duality and nonerasing quantum erasure," *Phys. Rev. A* **60**, pp. 4285–4290, Dec 1999.
10. S. P. Walborn, M. O. Terra Cunha, S. Pádua, and C. H. Monken, "Double-slit quantum eraser," *Phys. Rev. A* **65**, p. 033818, Feb 2002.
11. E. F. Taylor and D. F. Styer, "cT executor program version 3.0." `www.eftaylor.com/download.html#quantum`, June 2000.
12. N. J. Gunther, "Quantum design rules for optical engineers." `http://www.ewh.ieee.org/r6/scv/leos/archive/leosabs20060307.htm`, March 2006.
13. M. D. Abramoff, P. J. Magelhaes, and S. J. Ram, "Image processing with ImageJ," *Biophotonics International* **11**(7), pp. 36–42, 2004.
14. D. N. Klyshko, "Effect of focusing on photon-correlation in parametric scattering of light," *Zhurnal Eksperimentalnoi I Teoreticheskoi Fiziki* **94**(6), pp. 82–90, 1988. Sov. Phys. JETP, 87, 6, 1131–1135, June 1988.
15. M. D'Angelo and Y. Shih, "Quantum imaging," *Laser Physics* **Special issue**, 2005.
16. D. V. Strekalov, A. V. Sergienko, D. N. Klyshko, and Y. H. Shih, "Observation of two-photon "ghost" interference and diffraction," *Phys. Rev. Lett.* **74**, pp. 3600–3603, May 1995.
17. A. V. Sergienko, Y. Shih, T. B. Pittman, D. V. Strekalov, and D. N. Klyshko, "Two-photon geometric optical imaging and quantum cryptofax," *Proc. SPIE Int. Soc. Opt. Eng.*(2799), p. 164, 1996.
18. R. H. Haitz, "Studies on optical coupling between silicon p-n junctions," *Solid State Electronics* **8**, pp. 417–425, 1965.
19. A. Lacaita, M. Ghioni, and S. Cova, "Double epitaxy improves single-photon avalanche diode performance," *Electronics Letters* **25**(13), pp. 841–843, 1989.
20. A. Rochas, *Single Photon Avalanche Diodes in CMOS technology*. PhD thesis, EPFL, Lausanne, Switzerland, 2003.
21. D. Mosconi, D. Stoppa, L. Pacheri, L. Gonzo, and A. Simoni, "CMOS single-photon avalanche diode array for time-resolved fluorescence detection," *Proc. ESSCIRC*, October 2006. To appear.
22. C. Niclass and E. Charbon, "A single photon detector array with 64×64 resolution and millimetric depth accuracy for 3D imaging," *Proc. ISSCC* , pp. 364–365, February 2005.
23. C. Niclass, A. Rochas, P.-A. Besse, and E. Charbon, "Design and characterization of a cmos 3-d image sensor based on single photon avalanche diodes," *IEEE Journal of Solid-State Circuits* **40**, pp. 1847–1854, September 2005.
24. C. Niclass, M. Sergio, and E. Charbon, "A single photon avalanche diode array fabricated on deep-submicron CMOS technology," *Design and Test in Europe* , March 2004.
25. C. Niclass, M. Sergio, and E. Charbon, "A CMOS 64×48 single photon avalanche diode array with event-driven readout," *Proc. ESSCIRC*, October 2006. To appear.
26. B. F. Aull, A. H. Loomis, D. J. Young, R. M. Heinrichs, B. J. Felton, P. J. Daniels, and D. J. Landers, "Geiger-mode avalanche photodiodes for three dimensional imaging," *Lincoln Laboratory Journal* **13**(2), pp. 335–350, 2002.